SCIENCE CHINA
Life Sciences

THEMATIC ISSUE: Nanotechnology and nanomedicine
•RESEARCH PAPER•

April 2018 Vol.61 No.4: 436–447
https://doi.org/10.1007/s11427-017-9274-9

Synthesis and evaluation of a paclitaxel-binding polymeric micelle for efficient breast cancer therapy

Jiajia Xiang†, Bihan Wu†, Zhuxian Zhou*, Shiqi Hu, Ying Piao, Quan Zhou, Guowei Wang, Jianbin Tang, Xiangrui Liu & Youqing Shen*

Key Laboratory of Biomass Chemical Engineering of Ministry of Education, Center for Bionanoengineering, and College of Chemical and Biological Engineering, Zhejiang University, Hangzhou 310027, China

Received November 10, 2017; accepted December 15, 2017; published online March 19, 2018

Paclitaxel (PTX) is one of the most effective anticancer drugs for the treatment of various solid tumors, but its clinical use is limited by its poor solubility, low bioavailability, and severe systemic toxicity. Encapsulation of PTX in polymeric nanoparticles is used to overcome these problems but these micelles still need improvements in stability, pharmacokinetics, therapeutic efficacy, and safety profiles. In this study, we demonstrate a facile fabrication of a stable PTX-binding micelle made from poly (ethylene glycol)-*block*-dendritic polylysine, whose primary amines were reacted with phenethyl isothiocyanate (PEITC), a hydrophobic anticancer agent under clinical study. The amphiphilic conjugate (PEG-Gx-PEITC; Gx, the generation of the polylysine dendron) formed well-defined micelles whose core was composed of phenyl groups and thiourea groups binding PTX via π-π stacking and hydrogen bonding. Compared with the PTX-loaded poly(ethylene glycol)-*block*-poly(*D*,*L*-lactide) (PEG-PDLLA/PTX) micelles in clinical use, PTX-loaded PEG-Gx-PEITC third-generation (PEG-G3-PEITC/PTX) micelles showed slowed blood clearance, enhanced tumor accumulation, and thus much improved *in vivo* therapeutic efficacy in both subcutaneous and orthotopic human breast cancer xenografts. Therefore, PEG-G3-PEITC is a promising drug delivery system for PTX in the treatment of breast cancer.

paclitaxel delivery, paclitaxel-binding, phenethyl isothiocyanate, dendritic polylysine, polymeric micelles, cancer drug delivery, enhanced stability, prolonged blood circulation

Citation: Xiang, J., Wu, B., Zhou, Z., Hu, S., Piao, Y., Zhou, Q., Wang, G., Tang, J., Liu, X., and Shen, Y. (2018). Synthesis and evaluation of a paclitaxel-binding polymeric micelle for efficient breast cancer therapy. Sci China Life Sci 61, 436–447. https://doi.org/10.1007/s11427-017-9274-9

INTRODUCTION

Paclitaxel (PTX), a highly aqueous insoluble agent, is a broad-spectrum first-line chemotherapeutic agent for the treatment of metastatic breast cancer, refractory ovarian cancer, and other types of cancer. However, its clinical use is restricted because of the significant adverse effects of PTX itself and of the toxic vehicle solvent Cremophor EL in its commercial formulation (Taxol) (Singla et al., 2002).

To date, great efforts have been made for PTX delivery, but only a few Cremophor EL-free PTX polymeric micelles such as Genexol-PM and NK105 have entered the clinical trial stage (Tang et al., 2016). Notably, Genexol-PM is a polymeric micellar formulation made by self-assembly of PTX and poly(ethylene glycol)-*block*-poly(*D*,*L*-lactide) (mPEG-PDLLA) that was introduced in Korea in February 2007. It had a high maximum tolerable dose (MTD) and enhanced tumor accumulation. However, in preclinical study, the area under the curve (AUC) and blood circulation time of Genexol-PM were inferior to those of Taxol (Kim et al., 2001). This may result from the instability of the mPEG-PDLLA

†Contributed equally to this work
*Corresponding authors (Zhuxian Zhou, email: zhouzx@zju.edu.cn; Youqing Shen, email: shenyq@zju.edu.cn)

micelles and the weak interaction of PTX with PDLLA, causing burst release of the drug into the bloodstream shortly after intravenous administration (Chen et al., 2008; Stirland et al., 2013). Meanwhile, stability and long-blood circulating time are essential for a delivery system to extravasate from the bloodstream and preferentially accumulate in tumor tissue (Sun et al., 2012; Zhou et al., 2017; Zhu et al., 2015). Therefore, it is critical to develop PTX delivery systems with enhanced stability and prolonged blood time to further improve its therapeutic efficacy.

We proposed to develop a structurally well-defined linear-dendritic amphiphile forming strong PTX-binding micelle to improve the stability and blood circulation of the delivery system (Figure 1). The poly(ethylene glycol)-*block*-dendritic polylysine (PEG-DPLL) was chosen because DPLL made of natural *L*-lysine is biocompatible, biodegradable, and widely used for drug (Zhou et al., 2013) and gene delivery (Zhao et al., 2016). Phenethyl isothiocyanate (PEITC) was used as a hydrophobic moiety to modify DPLL. PEITC is a natural compound in cruciferous vegetables that is shown to have anticancer activity by suppressing cancer tumorigenesis and progression (Gupta et al., 2014; Wu et al., 2009). The click reaction of isothiocyanate (R-NCS) with the amines in DPLL dendron makes the conjugation facile and produces thiourea groups (Berglund et al., 2008), which act as H-bond acceptors to form intermolecular C=S···H–X hydrogen bonds with PTX (Saeed et al., 2015). More importantly, PEITC moieties can further bind PTX via π-π interactions between phenyl groups (Carstens et al., 2008). The two interactions together may improve the drug loading and the micelle stability for enhanced *in vivo* stability. Furthermore, some thiourea derivatives exert inherent and potent *in vivo* anticancer activity (Shao et al., 2017), which may generate a synergistic effect with the carried drugs.

Herein, we show that in comparison with commercial PEG-PDLLA/PTX, the PTX-loaded PEG-Gx-PEITC of third generation (PEG-G3-PEITC/PTX) micelles had good drug loading efficiency, slowed blood clearance, and enhanced tumor accumulation, producing much improved *in vivo* therapeutic efficacy in both subcutaneous and orthotopic human breast cancer xenografts.

RESULTS

Synthesis and characterization of polymers

PEG-DPLL of third and fourth generation were prepared and conjugated with stoichiometric amounts of PEITC to obtain PEG-G3-PEITC and PEG-G4-PEITC. The structures of the conjugates were confirmed by ^{1}H nuclear magnetic resonance (NMR) (Figure 2A and Figure S1 in Supporting Information), matrix-assisted laser desorption/ionization time-of-flight mass spectrometry (MALDI-TOF MS) (Figure 2B) and gel permeation chromatography (GPC) (Figure 2C). The average numbers of PEITC molecules attached to PEG-G3 and PEG-G4 were 7.6 and 15.6, respectively, as calculated from the ^{1}H NMR spectra from the integration ratio of the peaks at 2.71 to 2.86 ppm (–NHCH_2–, lysine) and 7.12 to 7.40 ppm (–*Ar*, PEITC). The number-average molecular weights of PEG-G3-PEITC and PEG-G4-PEITC measured by MALDI-TOF MS were 7,146.4 and 9,251.6 Da, respectively, which were consistent with the theoretical mass values of 7,142.7 and 9,484.0 Da. The GPC traces of both conjugates showed a single peak with a narrow and symmetrical distribution. The calculated number-average molecular weights (M_n) relative to polystyrene standard were 16,000 and 18,000 Da with polydispersity indices (PDI) of 1.06 and 1.09 for PEG-G3-PEITC and PEG-G4-PEITC, respectively. The molecular weights measured by GPC were much higher than the theoretical values due to the significant difference in the structures of the linear-dendritic polymers and the PS standard. The characterizations and properties of PEG-G3-PEITC and PEG-G4-PEITC are summarized in Table 1.

Preparation and characterizations of PTX-loaded micelles

The PTX-loaded micelles of PEG-Gx-PEITC were obtained by the solvent evaporation method (Tyrrell et al., 2010; Xiao et al., 2009) and the characterizations of the micelles are summarized in Table 1. The PEG-Gx-PEITC easily formed micelles in solution with PEG on the surface and Gx-PEITC in the core. The volume-average hydrodynamic sizes of PEG-G3-PEITC and PEG-G4-PEITC measured by DLS were 28 and 62 nm, respectively. The interior core of the PEG-Gx-PEITC micelles consisted of phenyl groups from PEITC moieties, which could form strong π-π stacking interactions with the benzene rings of PTX (Carstens et al., 2008; Xi et al., 2016). Moreover, the thiourea groups are likely to form hydrogen bonds with PTX (Saeed et al., 2015). So, PTX was efficiently encapsulated in the micelle core. The PEG-G3-PEITC micelles had a very high PTX encapsulation efficiency (98.3%) at a drug content of 23.7%. Loading PTX into the PEG-G3-PEITC micelles slightly increased the size to 31 nm with a PDI of as low as 0.13 (Figure 3A), which was further confirmed by the transmission electron microscopy (TEM) images (Figure 3B). Surprisingly, PEG-G4-PEITC micelles had a much lower PTX encapsulation efficiency and drug content than the PEG-G3-PEITC micelles (Table 1) possibly due to the self-packing of the PEITC phenyl groups.

Thus, PEG-G3-PEITC/PTX micelles were selected for further study. Their stability was evaluated by incubation with 10% fetal bovine serum (FBS) at 37°C. No substantial increase in size was detected after 72 h of incubation (Figure

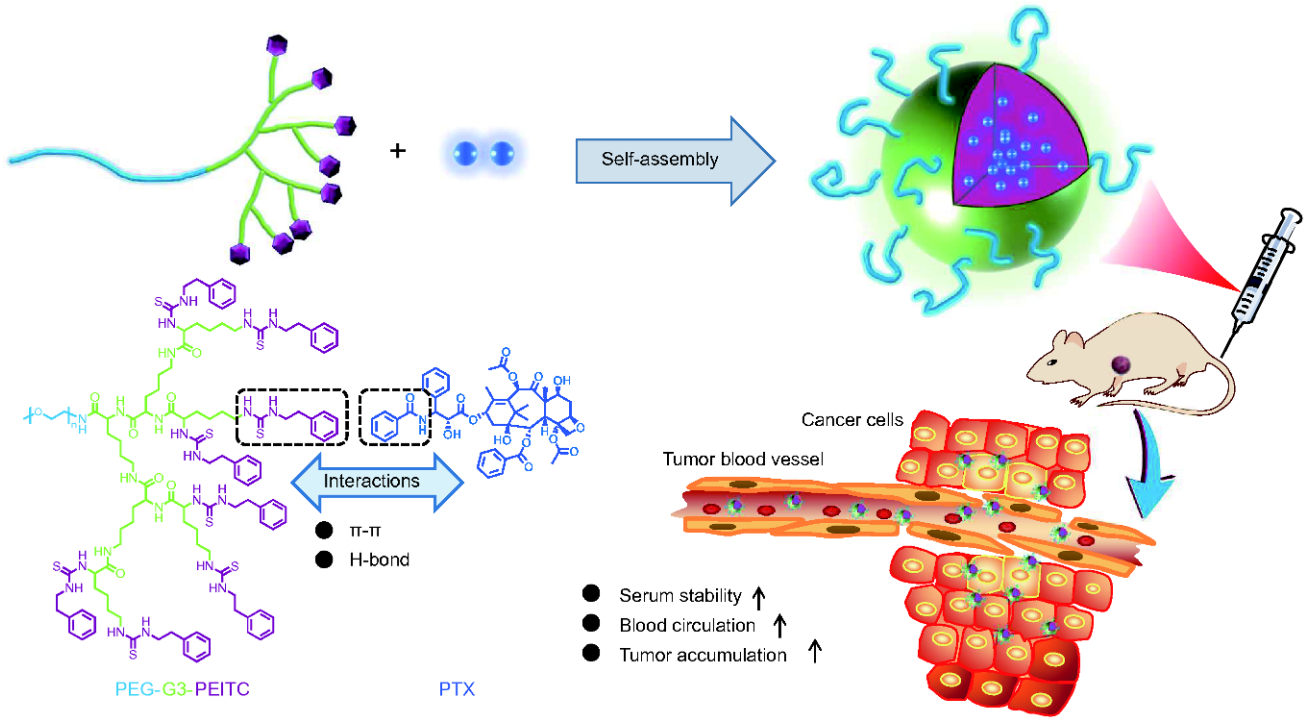

Figure 1 Schematic representation of self-assembly of PTX-binding polymeric micelles and the intermolecular interaction between drug and carrier. PEG-G3-PEITC/PTX micelles have improved serum stability, slowed blood clearance, and enhanced tumor accumulation.

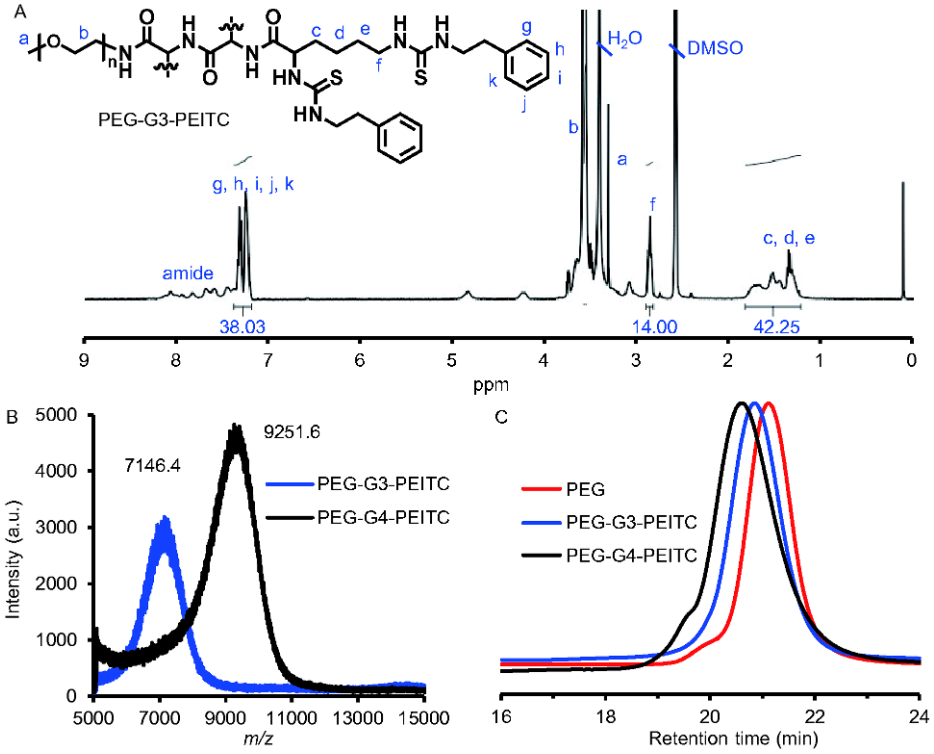

Figure 2 Characterizations of PEG-Gx-PEITC. A, ^{1}H NMR spectrum of PEG-G3-PEITC measured in DMSO-d_6. B, MALDI-TOF MS spectra. C, GPC traces (DMF, 50°C, 0.8 mL min^{-1}).

S3A in Supporting Information), which suggests great stability of the micelles. No increase in absorbance occurred after 36 h of incubation, indicating PEG-G3-PEITC/PTX micelles were stable in 50% FBS and 100% FBS (Figure S3B in Supporting Information). The lyophilization and reconstitution of PEG-G3-PEITC/PTX micelles were

Table 1 Characterizations of polymers and PTX-loaded micelles[a)]

Polymers	PEG-G3-PEITC	PEG-G4-PEITC	PEG-PDLLA
Block length*	5,000:2,143	5,000:4,484	2,000:2,000
m/z**	7,146.4	9,251.6	–
$M_{n,\ GPC}$	16,000	18,000	–
$M_{w,\ GPC}$	17,000	20,000	–
PDI***	1.06	1.09	–
CMC (mg mL^{-1})****	0.031	0.025	0.036
Size of blank micelles (nm)*****	28	62	24
Size of PTX-loaded micelles (nm)*****	31	72	39
PDI*****	0.13	0.31	0.24
Zeta potential (mV)	−6.69	−4.03	−4.85
PTX loading content (wt.%)******	23.7	5.6	22.8
Encapsulation efficiency (wt.%)******	98.3	52.1	97.4

a) *, Determined by ^{1}H NMR spectra. **, Determined by MALDI-TOF MS. ***, Polydispersity index (PDI) obtained by GPC. ****, Critical micelle concentration (CMC) was measured with a Nile red fluorescent method (Figure S2 in Supporting Information). *****, Measured by dynamic light scattering (DLS). ******, PTX content was determined by high-performance liquid chromatography (HPLC).

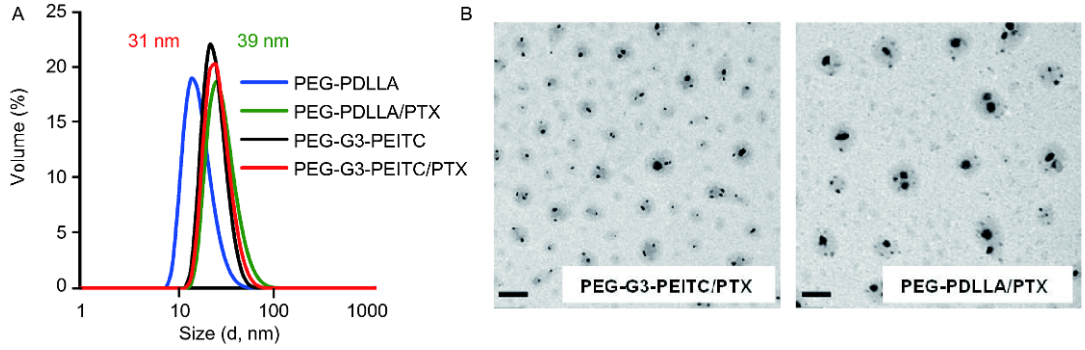

Figure 3 Characterizations of micelles. A, Sizes of PEG-G3-PEITC blank micelles, PEG-G3-PEITC/PTX, PEG-PDLLA blank micelles, and PEG-PDLLA/PTX measured by DLS in phosphate-buffered saline solution (PBS). B, TEM images of micelles. Scale bar, 200 nm.

evaluated for its importance in clinical practice. Freeze-dried PEG-G3-PEITC/PTX micelles with 2% mannitol were obtained as white powder and could be easily redissolved in aqueous media to form stable micelles with unchanged size (Figure S3C in Supporting Information).

PEG-PDLLA/PTX, clinically used PTX-loaded polymeric micelles, were used as a control system and obtained as reported in the literature (Kim et al., 2001). The micelles were approximately 39 nm and had a PTX loading content of 23.7%, which was in line with reported results (Kim et al., 2001). The characterizations of PEG-PDLLA/PTX micelles are summarized in Table 1.

Interactions between PEG-G3-PEITC and PTX

PEG-G3-PEITC exhibited a high PTX encapsulating efficiency and loading content possibly due to the potential π-π stacking interaction and hydrogen bond interaction between the PEITC moieties and PTX molecules. These interactions were studied by ^{1}H NMR, ^{13}C NMR, Fourier-transform infrared spectroscopy (FTIR) and X-ray powder diffraction (XRD). The ^{1}H NMR signals from PEG-G3-PEITC in DMSO-d_6 and PTX in $CDCl_3$ were palpable (Figure S4 in Supporting Information). Nevertheless, when the PEG-G3-PEITC/PTX micelles were dissolved in D_2O, all of the characteristic proton signals of PTX and PEG-G3-PEITC were suppressed except for the PEG signals (3.45 to 3.55 ppm), which indicated that the PTX was completely surrounded by PEG and encapsulated inside the hydrophobic core. The ^{13}C NMR spectra of PTX and PTX mixed with PEG-G3-PEITC (molar ratio, 1:2) were recorded in $CDCl_3$ (Figure 4A). The chemical shifts of PTX mixed with PEG-G3-PEITC changed. The signal shift index (Δ) was defined as the net change of the chemical shift of a carbon atom relative to that of the free PTX. Sum was calculated as cumulative absolute values of the changes of all the benzene-ring carbon atoms' chemical shifts. It was suggested a shift of more than 0.02 in ^{13}C NMR indicates intermolecular interactions (Zhang et al., 2014; Zhang et al., 2015). The signal shifts of the carbon atoms in the three benzene-rings of PTX

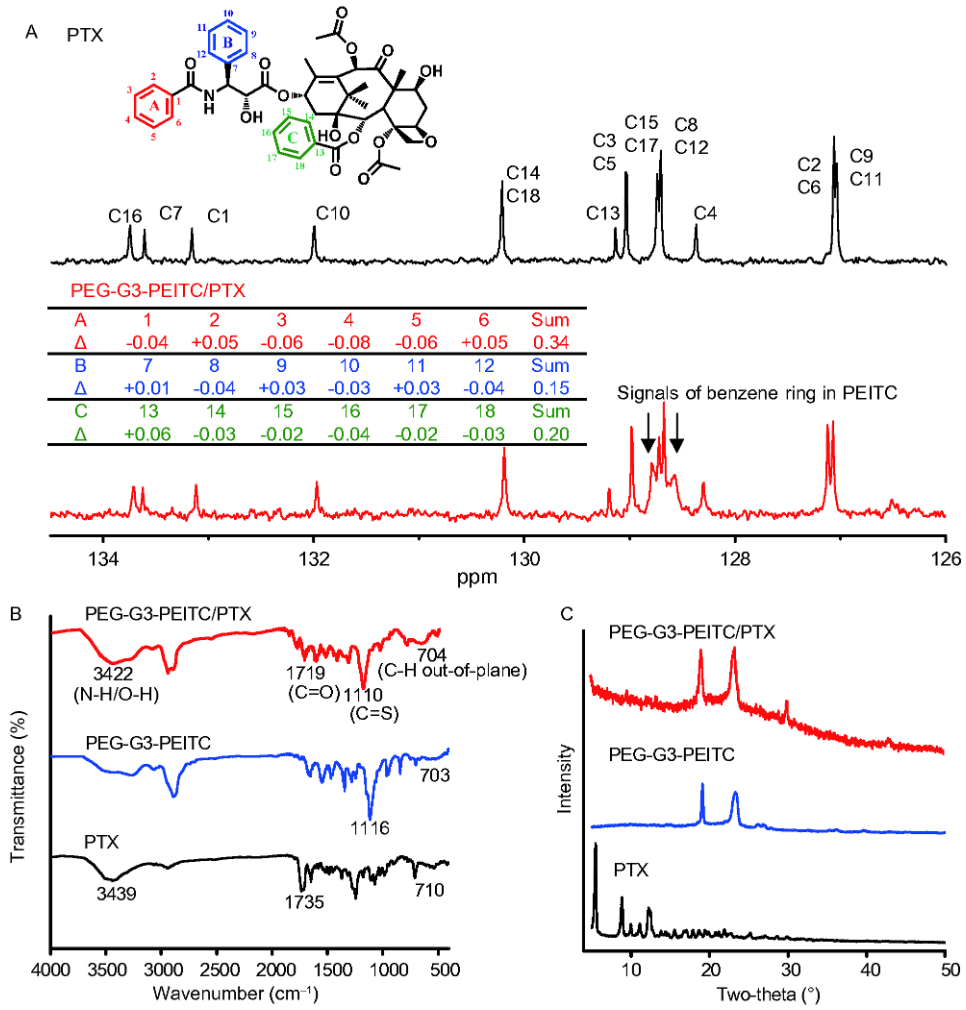

Figure 4 Study of interactions between PEG-G3-PEITC and PTX. A, ^{13}C NMR of PTX and PTX mixed with PEG-G3-PEITC in $CDCl_3$. The signal shift index (Δ) was defined as the chemical shift change of the carbon atom before and after mixing with carriers compared with free PTX. Sum was calculated as cumulative absolute values of the changes of all the benzene-ring carbon atoms' chemical shifts. PTX was mixed with PEG-G3-PEITC at a molar ratio of 1:2 in accordance with the ratio in micelles. B, Fourier-transform infrared analysis (FTIR) spectra of PTX, PEG-G3-PEITC, and PEG-G3-PEITC/PTX micelles. C, X-ray diffraction (XRD) patterns of PTX, PEG-G3-PEITC, and PEG-G3-PEITC/PTX micelles.

were compared with free PTX. The cumulative sums of the changes of rings A, B, and C were 0.34, 0.15, and 0.20, respectively. Ring A of PTX showed a larger change than rings B and C. These preliminary data demonstrated π-π interactions of aromatic rings between the dendritic core and PTX in PEG-G3-PEITC/PTX micelles.

We further used FTIR to characterize the interaction of PTX and PEITC in the PEG-G3-PEITC/PTX micelles (Figure 4B). By comparing the spectra of PTX, PEG-G3-PEITC with PEG-G3-PEITC/PTX, remarkable changes were found in the regions of 2,800–3,600 cm^{-1} and 500–1,900 cm^{-1}, indicating strong hydrogen bond and π-π interactions. The obvious blueshift of C=S stretching frequency from 1,116 to 1,110 cm^{-1}, N–H and O–H absorption bands from 3,439 to 3,422 cm^{-1}, indicated the formation of strong hydrogen bonds between C=S and X–H. The result is in line with the previous report that C=S group can act as H-bond acceptors and form intermolecular C=S···H–X hydrogen bond (Saeed et al., 2015). Moreover, the C–H out-of-plane bend of the benzene ring at 710 cm^{-1} and C=O stretching frequency at 1,735 cm^{-1} were both weaker in the spectrum of PEG-G3-PEITC/PTX micelles, further indicating the existence of π-π interactions and hydrogen bond interactions between PTX and PEITC moieties (Mishra et al., 2014; Muthoosamy et al., 2016; Tang et al., 2014).

To evaluate the dispersion state of PTX in micelles, XRD analysis was performed on PTX, PEG-G3-PEITC, and PEG-G3-PEITC/PTX micelles, and their diffractograms are shown in Figure 4C. PTX is a highly crystalline drug which exhibited sharp and narrow peaks. In comparison, PEG-G3-PEITC/PTX showed flattened peaks, indicating that the loaded PTX was in an amorphous state. This result illustrated that potential drug/carrier interactions might inhibit PTX crystallization and thus increased the drug loading capability (Tang et al., 2014).

Taken together, drug/carrier interactions, including π-π

stacking and hydrogen bonds, may engage in the formation of PEG-G3-PEITC/PTX micelles and lead to high drug loading capability and enhanced stability (Guo et al., 2016).

In vitro release

The drug release profiles of the PEG-G3-PEITC/PTX and PEG-PDLLA/PTX micelles were monitored via a dialysis method in mediums of PBS (0.01 mol L^{-1}, pH 7.4 or 5.4) in a shaker (37°C, 100 r min^{-1}) (Figure 5). It is usually difficult to obtain a good sink condition for drugs such as PTX with poor water solubility. In this study, a good sink condition could be achieved for PTX by adding 0.5% tween 80 into the immersed mediums. Both micelles showed sustained release. At pH 7.4, PEG-G3-PEITC/PTX and PEG-PDLLA/PTX micelles had released about 50% and 70%, respectively, after 48 h. The PEG-G3-PEITC/PTX micelles showed better stability with a slower release than the PEG-PDLLA/PTX micelles. At pH 5.4, PEG-G3-PEITC/PTX and PEG-PDLLA/PTX micelles had released about 70% and 80%, respectively, after 48 h. The increased PTX release of PEG-G3-PEITC/PTX micelles at a low pH may be due to the weakened hydrogen bonds in acidic condition. This release feature is advantageous for cancer drug delivery, which may allow for preferential delivery of a drug into the acidic tumor extracellular fluid (pH 6 to 7) (Zhou et al., 2014).

In vitro cytotoxicity

The *in vitro* cytotoxicity of blank and PTX-loaded micelles was evaluated by MTT assay on HeLa, MCF-7, and MDA-MB-231 cancer cells. Blank micelles alone had negligible toxicity on cell proliferation, even at concentrations as high as 0.6 mg mL^{-1} (Figure S5 in Supporting Information). The PTX-loaded micelles showed dose-dependent inhibiting efficacy on different cancer cell lines, which was comparable to that of free PTX (Figure 6A–C). The IC_{50} values of PEG-G3-PEITC/PTX micelles, PEG-PDLLA/PTX micelles, and free PTX on HeLa cells were 0.244, 0.277, and 0.211 μg PTX mL^{-1}, respectively, whereas the IC_{50} values of these agents on MCF-7 cells were 0.012, 0.021, and 0.014 μg PTX mL^{-1}, respectively (Table 2). MCF-7 cells are more sensitive to PTX than HeLa cells. On MDA-MB-231 cells, the high concentrations of PTX did not further increase inhibition, similar to previous reports (Liu et al., 2013), which may be due to the improved DNA repair capacity of the MDA-MB-231 cells (Skog et al., 2004).

Pharmacokinetics and biodistribution

The pharmacokinetics of PEG-G3-PEITC/PTX and PEG-PDLLA/PTX micelles were studied after single-dose intravenous injection at an equivalent PTX dose of 10 mg kg^{-1} into ICR mice (n=3). As shown in Figure 7A, PEG-G3-PEITC/PTX micelles had a relatively slow clearance from the blood. A pharmacokinetics analysis using a two-compartment model was performed for both formulations (Table 3) (Wei et al., 2014; Zhao et al., 2015). The PEG-G3-PEITC/PTX micelles exhibited more favorable pharmacokinetics than the PEG-PDLLA/PTX micelles, with around 1.7-fold longer half-life ($T_{1/2}$) and two-fold larger AUC (P<0.05). Hence, the PEG-G3-PEITC/PTX micelles had a more propitious pharmacokinetics profile for tumor drug accumulation.

In vivo real-time drug distribution was tracked on BALB/c nude mice bearing MCF-7 tumors and visualized with near-infrared fluorescence imaging (Figure 7B). PEG-PDLLA/PTX and PEG-G3-PEITC/PTX micelles were covalently labeled with Cy5. The distribution of two micelles was similar within the first 2 h post-injection. High fluorescence intensity was observed throughout whole body and gradually accumulated in the tumor sites. After 5 h, both of the micelles showed much higher accumulation in tumor site than in other sites. High fluorescence contrast between tumors and surrounding tissues was observed and sustained throughout the following experimental period. For the PEG-PDLLA/PTX-treated group, strong fluorescence intensity was observed in the bladder at 8 and 12 h post-injection, probably due to the dissociation of micelles into free polymers and thus rapid clearance via renal excretion (Burt et al., 1999). Over the same time period, no obvious increased fluorescence intensity was observed in the bladder of mice injected with PEG-G3-PEIT/PTX, which indicated its relatively high stability. The enhanced stability of PEG-G3-PEIT/PTX resulted in more sustained and higher level of fluorescence intensity throughout the whole body, in consistent with its relatively long circulation time as shown in Figure 7A. Compared to PEG-PDLLA/PTX micelles, PEG-G3-PEITC/PTX micelles also showed higher tumor accumulation.

In vivo antitumor experiment

The *in vivo* antitumor activity of the PTX formulations was first studied via intravenous injection in mice with subcutaneous MCF-7 tumors (Figure 8A and B). PEG-G3-PEITC/PTX or PEG-PDLLA/PTX micelles were administered at a PTX dose of 10 mg kg^{-1} every other day. Compared to the PBS group, both PEG-G3-PEITC/PTX and PEG-PDLLA/PTX micelles treatments greatly slowed the tumor growth rates, and no significant difference was observed during the treatment period. Notably, significant difference was observed during the treatment-free period. Tumors of mice treated with PEG-PDLLA/PTX micelles relapsed quickly from day 18, while no obvious tumor relapse was observed on mice treated with PEG-G3-PEITC/

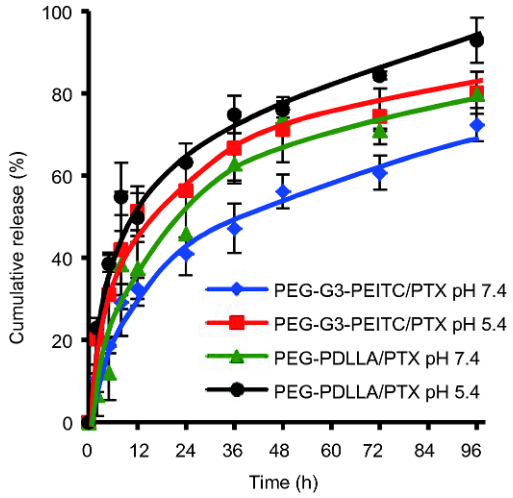

Figure 5 The drug release profiles of PEG-G3-PEITC/PTX and PEG-PDLLA/PTX micelles in mediums of PBS (0.01 mol L^{-1}, pH 7.4 or 5.4). Data are depicted as mean±SD.

PTX micelles during the experimental period. The PEG-G3-PEITC/PTX micelles had a tumor inhibition rate (IR) of 90% (P<0.0005) at the experiment's end. PEG-G3-PEITC/PTX micelles showed significantly higher antitumor efficacy than PEG-PDLLA/PTX (P<0.05). Remarkably, after treatment with PEG-G3-PEITC/PTX micelles, tumors were completely eradicated in three of the five PEG-G3-PEITC/PTX-treated mice, which remained tumor-free thereafter. In comparison, only one mouse was free of tumor after the treatment of PEG-PDLLA/PTX micelles. The body weights of all mice did not change significantly (Figure S6A in Supporting Information). No other noticeable symptoms of side effects, abnormal behaviors, or impaired movements were observed during the treatment.

The antitumor efficacy of PEG-G3-PEITC/PTX and PEG-PDLLA/PTX micelles was also evaluated on mice bearing mammary fat pad-inoculated orthotopic MDA-MB-231, a highly metastatic human triple-negative breast cancer cell line (Yano et al., 2016), and the result is illustrated in Figure 8C and D. Both PTX formulations showed significant tumor suppression effect compared to PBS. During the treatment-free period, an increase in tumor volume in PEG-PDLLA/PTX-treated mice was observed, while significant inhibition of tumor growth could be observed with the treatment of PEG-G3-PEITC/PTX micelles. At the experiment's end, the PEG-G3-PEITC/PTX micelles had a tumor IR of 90% (P<0.0005). PEG-G3-PEITC/PTX micelles effectively suppressed tumor growth compared to the PEG-PDLLA/PTX micelles (P<0.05). The body weights of all mice remained nearly unchanged throughout the experimental period, and none of the mice exhibited overt signs of toxicity (Figure S6B in Supporting Information). These results indicated that PEG-G3-PEITC/PTX micelles exhibited much better antitumor activity than PEG-PDLLA/PTX micelles. Furthermore, hematoxylin and eosin (H&E) stained sections of tumors, hearts, livers, spleens, lungs, and kidneys were obtained for examination of tissue morphology. The tumors of the PBS group were composed of tightly packed tumor cells. While in PEG-G3-PEITC/PTX and PEG-PDLLA/PTX micelles treated group, nuclear shrinkage and extensive cellular changes in many cancer cells were observed, indicating

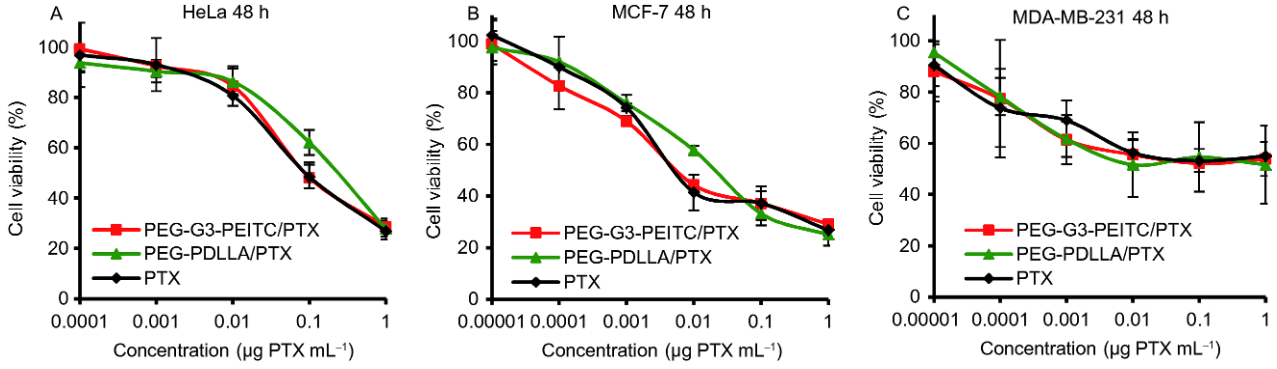

Figure 6 *In vitro* cytotoxicity. Cytotoxicity of PEG-G3-PEITC/PTX, PEG-PDLLA/PTX micelles, and PTX against HeLa (A), MCF-7 (B), and MDA-MB-231 cells (C) after 48 h incubation. Data are depicted as mean±SD (n=6).

Table 2 IC_{50} of PEG-G3-PEITC/PTX, PEG-PDLLA/PTX micelles, and PTX on different cancer cell lines.

Formulation	IC_{50} (μg PTX mL^{-1})		
	HeLa	MCF-7	MDA-MB-231
PEG-G3-PEITC/PTX	0.244	0.012	>1
PEG-PDLLA/PTX	0.277	0.021	>1
PTX	0.211	0.014	>1

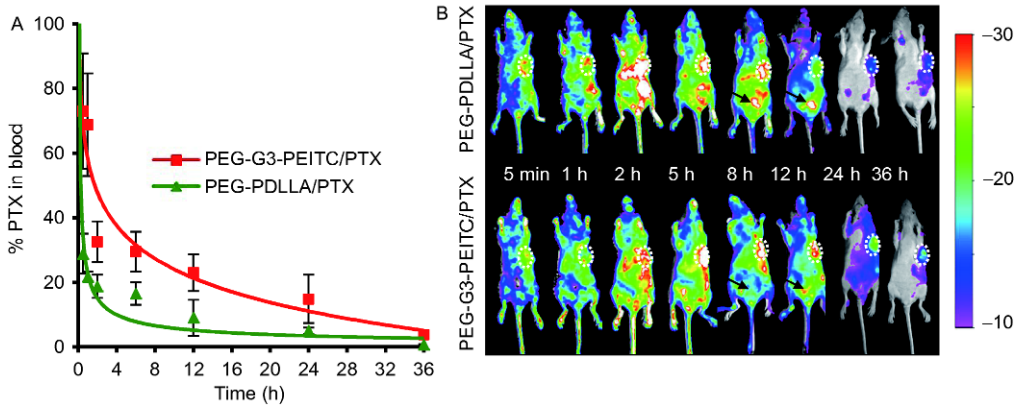

Figure 7 Plasma pharmacokinetic profiles and biodistribution. A, Blood clearance profiles of PEG-PDLLA/PTX and PEG-G3-PEITC/PTX micelles. ICR mice (n=3) received an equivalent dose of 10 mg kg^{-1} PTX by intravenous injection. Blood samples were collected at 3 min and 0.5, 1, 2, 6, 12, 24 and 36 h. The concentration in the plasma was normalized as the percentage of PTX concentration at 3 min. Data are depicted as mean±SD. B, *In vivo* real-time biodistribution study. Nude mice bearing MCF-7 tumors received Cy5-labeled micelles (eq. 10 mg kg^{-1} PTX). Animals under anesthesia underwent imaging at predetermined intervals after injection (5 min and 1, 2, 5, 8, 12, 24 and 36 h). Dotted circle outlines the tumor. The urinary bladder is indicated by arrows.

Table 3 Pharmacokinetic parameters of PEG-PDLLA/PTX and PEG-G3-PEITC/PTX micelles (ICR mice, n=3, intravenously, eq. 10 mg kg^{-1} PTX)[a)]

Parameter	Unit	PEG-PDLLA/PTX	PEG-G3-PEITC/PTX
$T_{1/2}$ alpha	h	0.12±0.04	0.27±0.17
$T_{1/2}$ beta	h	10.42±1.58	16.85±4.29
AUC_{0-t}	μg mL^{-1} h^{-1}	220.92±34.86	445.83±178.08*

a) $T_{1/2}$ alpha: half-life of distribution phase. $T_{1/2}$ beta: half-life of elimination phases. Data are depicted as mean±SD. Statistical significance: *, P<0.05.

apoptosis in cancer cells (Figure 8E). Neither obvious histopathologic abnormalities nor impairments were observed in any major organs after treatment (Figure S7 in Supporting Information). These results verified the safety and biocompatibility of PEG-G3-PEITC/PTX and PEG-PDLLA/PTX micelles. Therefore, PTX delivery via PEG-G3-PEITC achieved high anticancer efficiency and low toxicity.

CONCLUSION

We developed a well-defined linear-dendritic conjugate, PEG-G3-PEITC, for effective encapsulation of PTX and efficient anticancer drug delivery. The amphiphilic conjugate self-assembled into stable micelle in aqueous solution and efficiently encapsulated PTX. The PEITC moieties in the micelle formed strong π-π interactions and hydrogen bonds with PTX molecules. The PEG-G3-PEITC/PTX micelles showed similar *in vitro* cytotoxicity with the clinically used PEG-PDLLA/PTX micelles and free PTX, but exhibited slowed blood clearance, enhanced tumor accumulation, and thus much improved *in vivo* therapeutic efficacy in both subcutaneous and orthotopic breast cancer xenografts, as well as low toxicity. Therefore, PEG-G3-PEITC/PTX has a great promise for efficient breast cancer therapy.

MATERIALS AND METHODS

Materials, cell lines and animals

Amine terminated methoxypoly(ethylene glycol) with a molecular weight of ~5,000 ($mPEG_{5K}$-NH_2) was purchased from Yarebio (Shanghai). Boc-Lys(Boc)-OH, trifluoroacetic acid (TFA), *N*-hydroxysuccinimide (NHS), *N*,*N*-dicyclohexylcarbodiimide (DCC), phenethyl isothiocyanate (PEITC), 2,3,4,5,6-pentafluorophenol (PFP), *N*,*N*-diisopropylethylamine (DIPEA) and 4-(dimethylamino)pyridine (DMAP) were purchased from Energy Chemical (Shanghai). PEG-PDLLA was purchased from Daigang Biomaterial Co., Ltd. (Jinan). 3-(4,5-Dimethylthiazolyl-2)-2,5-diphenyltetrazolium bromide (MTT) was purchased from Sigma-Aldrich (USA). Paclitaxel (PTX, >99%) was purchased from Huilin Bio-tech Co., Ltd. (Xi'an, China). All the organic solvents were purchased from Sinopharm Chemical Reagent Co., Ltd. (Shanghai). *N*,*N*-dimethylformamide (DMF), dichloromethane (DCM) and tetrahydrofuran (THF) were dried with CaH_2 and distilled. PEG-dendritic polylysines of different generations (PEG-G3 and PEG-G4) were synthesized according to the previously reported method (Zhou et al., 2013). All cancer cell lines were obtained from the American Type Culture Collection (ATCC). Human breast cancer cells MCF-7, cervical cancer cells HeLa and triple-negative human breast cancer cells MDA-MB-231 were cultured in 1640 medium with 10% FBS (Gibco, USA) and

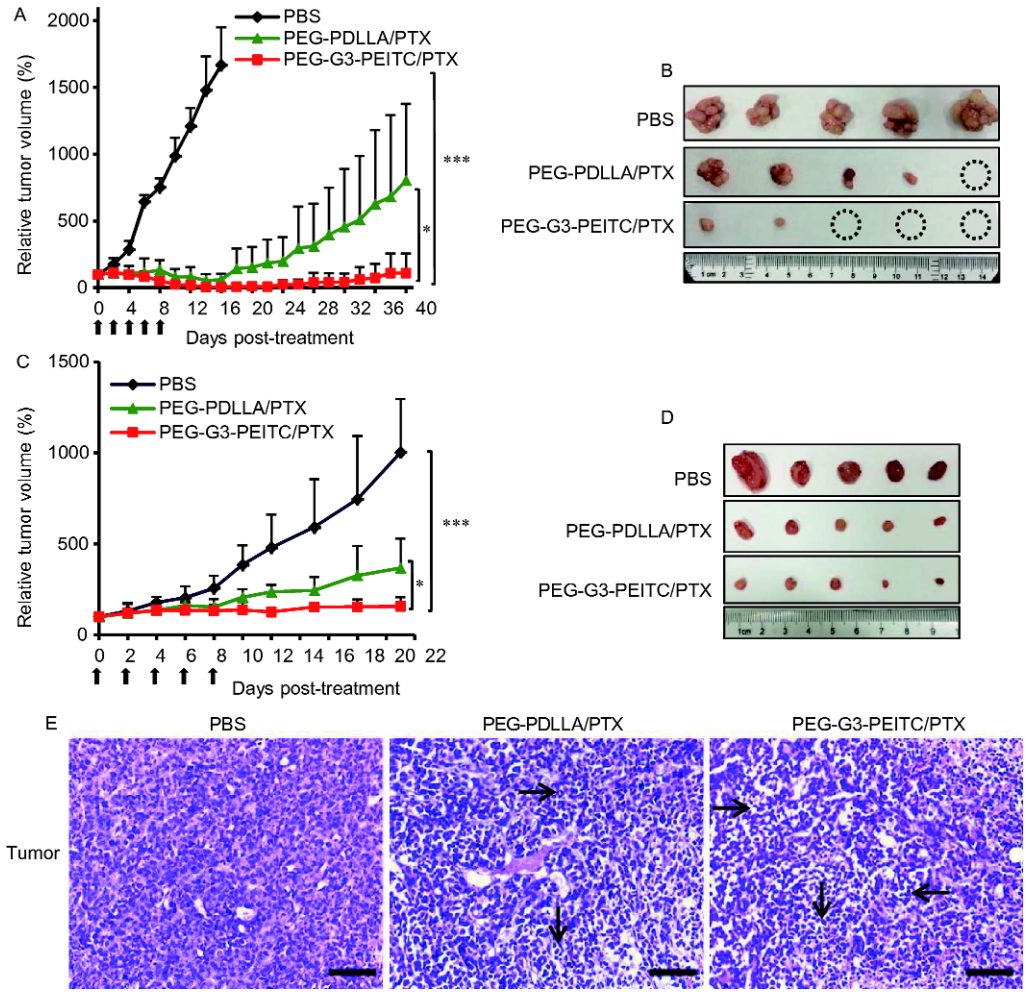

Figure 8 Antitumor effect. Nude mice with MCF-7 or MDA-MB-231 tumors received PBS, PEG-PDLLA/PTX, or PEG-G3-PEITC/PTX micelles (n=5, q2×5, eq. 10 mg kg^{-1} PTX). Dosing schedules are indicated by black arrows. A, Tumor volumes as a function of time for mice with MCF-7 tumors. B, Images of MCF-7 tumors at the end of the experiment. Dotted circle represents mice which were tumor-free. C, Tumor volumes as a function of time for mice with MDA-MB-231 tumors. D, Images of MDA-MB-231 tumors harvested at the end of the experiment. E, Histologic features of MDA-MB-231 tumors. Tissue paraffin sections were stained with hematoxylin-eosin (H&E) and examined by light microscopy. Tumor apoptosis is indicated by arrows. Data are depicted as mean±SD. Statistical significance: *, P<0.05; **, P<0.005, and ***, P<0.0005. Scale bar, 70 μm.

1% penicillin/streptomycin (Sigma-Aldrich). Female BALB/c homozygous athymic nude mice and ICR mice (6–8 weeks) were purchased from the Animal Center of Zhejiang University and maintained under standard conditions. Animal experiments were approved by the Animal Care and Use Committee of Zhejiang University and were carried out in accordance with the institutional guidelines.

Synthesis of PEG-G3-PEITC and PEG-G4-PEITC

PEG-G3 (500 mg, 0.073 mmol), PEITC (100 mg, 0.613 mmol), and trimethylamine (Et_3N, 162 μL) were mixed in dimethyl sulfoxide (DMSO, 4 mL) and stirred overnight at 45°C. The solution was dialyzed against methanol (MWCO=3,500) for 12 h. After removing the solvent under vacuum, the white product was obtained by precipitation in ether (20 mL×3) with a 90% yield. PEG-G4-PEITC was synthesized similarly. PEG-G3-PEITC: ^{1}H NMR (400 MHz, DMSO) δ=7.40–7.12 (m, 38H), 3.51 (s, 456H), 2.78 (t, J=7.0, 14H), 1.74–1.12 (m, 42H). PEG-G4-PEITC: ^{1}H NMR (400 MHz, DMSO) δ=7.29 (dd, J=45.5, 38.8, 78H), 3.51 (s, 456H), 2.78 (s, 30H), 1.79–1.11 (m, 92H).

Synthesis of Cy5-labeled PEG-G3-PEITC and PEG-PDLLA

PEG-G3 (10 mg) and Cyanine5-NHS ester (0.12 mg, Mirus Bio) were dissolved in DMSO (1 mL) and stirred overnight in the dark, followed by the addition of PEITC (2 mg, 0.012 mmol) and Et_3N (4 μL). After stirring for another 24 h, the solution was dialyzed against methanol (MWCO=3,500) for 24 h. Cy5 content was about 0.4% given by fluorescence intensity. PEG-PDLLA (0.5 g, 0.125 mmol) was dissolved in THF (5 mL) and succinic anhydride (0.1 g, 1 mmol) was added, followed by adding 2 mL of pyridine. After stirring at 45°C for 12 h, the product was obtained by precipitation in

diethyl ether thrice. The obtained PEG-PDLLA-COOH, NHS (0.15 g, 1.3 mmol), and DCC (0.2 g, 0.95 mmol) were dissolved in THF (10 mL) and stirred for 12 h at 45°C. Then ethylenediamine (0.05 mL, 0.75 mmol) was added and stirred for another 12 h. The resulting mixture was filtered, concentrated and the residue was redissolved in DCM (50 mL). The mixture was then washed with 0.1 mol L^{-1} HCl, saturated $NaHCO_3$ solution, and brine. After separation, the organic phase was dried over Na_2SO_4, concentrated, and precipitated in ether to give PEG-PDLLA-NH_2 as a white solid. Cy5-labeled PEG-PDLLA was obtained by the same method above.

CMC determination

The CMC of each polymer was determined by fluorescence method (Wang et al., 2013). Briefly, Nile red (10^{-4} mol L^{-1}, 20 μL) in DCM was put into each vial. The solvent was evaporated, and micelles (2 mL) were added with predetermined concentrations. Vials were stirred at 37°C for 12 h in the dark. The fluorescence emission intensity of each solution was measured at the wavelength of 620 nm (exited at 579 nm). The CMC was referred as the intersection of the two fitting straight-lines of emission intensity over polymer concentration.

Preparation of PTX-loaded micelles

A solvent evaporation method was applied for self-assembly of PTX-loaded micelles. PEG-G3-PEITC was dissolved in 1 mL of acetonitrile. Predetermined PTX was added, and the solution was evaporated under reduced pressure at 40°C to form a thin transparent gel-like film. Preheated water was added to re-hydrate with gentle stirring. PTX-loaded PEG-G4-PEITC or PEG-PDLLA micelles were obtained by the same method. The transparent PEG-G3-PEITC/PTX micelles solution was filtered through a 0.22 μm filter for the study of lyophilization and reconstitution. 2% mannitol was used as lyophilization protector.

Characterizations of micelles

The size of the micelles was determined by DLS with He-Ne laser light (632.8 nm) at 173° scattering angle. The zeta-potential was detected by a Nano-ZS Zetasizer (Malvern Instrument Ltd., UK). The morphology of the micelles was characterized by TEM. Briefly, micelles solution (1 mg mL^{-1}, 20 μL) was applied onto a copper grid and imaged on JEOL-1010 transmission electron microscope. 1% (*w*/*v*) aqueous uranyl acetate and 1% (*w*/*v*) phosphotungstic acid solutions were used as staining agents for PEG-PDLLA/PTX and PEG-G3-PEITC/PTX micelles, respectively. The amount of PTX was determined by reverse-phase HPLC (Waters, Singapore) with a C4 column (4.6 mm×250 mm, Waters, Ireland) heated at 35°C. UV detection was performed at 227 nm. The mobile phase consisted of HPLC grade acetonitrile/deionized water (60:40, v/v) delivered at a flow rate of 1.0 mL min^{-1}. Drug loading content and encapsulation efficiency of micelles were determined as follows.

Drug loading content%=Drug content in micelles/Weight of micelles×100%

Encapsulation efficiency%=Drug content in micelles/Feeding drug×100%

Stability of micelles was evaluated by incubating in 10% FBS at 37°C. Stability of reconstitution was monitored by DLS. An absorbance method was used to test the 50% FBS and 100% FBS stability of PEG-G3-PEITC/PTX micelles by measuring changes in absorbance at a wavelength of 560 nm (Fang et al., 2010). ^{1}H NMR spectra of PTX, PEG-G3-PEITC, and PEG-G3-PEITC/PTX micelles were tested in $CDCl_3$, DMSO-d_6, and D_2O, respectively. ^{13}C NMR spectra of PTX and PTX mixed with PEG-G3-PEITC were analyzed in $CDCl_3$. PTX was mixed with PEG-G3-PEITC at a molar ratio of 1:2 in accordance with the ratio in micelles.

FTIR

The characteristic bands of PTX, PEG-G3-PEITC, and PEG-G3-PEITC/PTX were obtained on a FTIR Nicolet iS50 system using KBr pellets method. Samples were scanned in the range 4000 to 400 cm^{-1}.

XRD

X-ray diffraction patterns of PTX, PEG-G3-PEITC, and PEG-G3-PEITC/PTX were analyzed on an X'Pert PRO diffractometer (PANalytical, the Netherlands). Samples were scanned at 40 kV and 40 mA with a scanning diffraction angle (2θ) of 5°–50° and step size of 0.02°.

Study of PTX release curves

Release of PTX from polymeric micelles was examined in sink mediums of PBS (0.01 mol L^{-1}, pH 7.4 or 5.4) solutions with 0.5% tween 80 (Wang et al., 2012). Micelles (eq. 1 mg mL^{-1} PTX, 0.6 mL) were placed into a dialysis bag (MWCO=3,500), and dialyzed against 50 mL mediums in a 37°C shaker with a speed of 100 r min^{-1}. Samples (100 μL) were taken at predetermined time intervals and equal volume mediums were added. The PTX concentrations were determined by HPLC and accumulative release ratios were calculated.

In vitro cytotoxicity

MCF-7, MDA-MB-231, and HeLa cells were used to study

the *in vitro* cytotoxicity. Cells (100 μL cell suspension, 5×10^3 cells well^{-1}) were plated in 96-well plates for 12 h incubation. After 48 h exposure of different agents, cells were incubated with medium containing 0.75 mg mL^{-1} MTT for 3 h. The medium was removed and DMSO (100 μL) was added to each well. The absorbance was calculated as the difference value of 562 and 620 nm measured by a microplate spectrophotometer (Molecular Devices, SpectraMax M2e, USA). Each test was performed six repetitions.

In vivo pharmacokinetics analysis

Female ICR mice (6–8 weeks) were injected intravenously (*i.v.*) through the tail vein with PEG-G3-PEITC/PTX or PEG-PDLLA/PTX micelles (n=3, eq. 10 mg kg^{-1} PTX). Blood samples were withdrawn from eyes retro-orbital plexus at timed intervals (3 min and 0.5, 1, 2, 6, 12, 24 and 36 h). Each plasma sample (50 μL) was mixed with acetonitrile (200 μL), and centrifuged at 600×g for 10 min to precipitate proteins. The supernatant (20 μL) was subject to HPLC analysis. Standard curve for PTX in blood was generated by adding free PTX to the whole blood. PTX was extracted and quantified as mentioned above.

In vivo antitumor efficacy

Female BALB/c nude mice (6–8 weeks) were inoculated subcutaneously (*s.c.*) into the right flank with MCF-7 cells suspensions (8×10^6 (200 μL)$^{-1}$ PBS). Treatments were started when tumor volume reached approximately 100 mm^3. This day was designated as day 0. Mice (n=5) were administered *i.v.* with PEG-G3-PEITC/PTX or PEG-PDLLA/PTX micelles at a dose of 10 mg kg^{-1} PTX every two days for five times. Body weight was recorded and tumor volume was calculated by the formula: tumor volume=(width^2× length)/2. Relative tumor volume was calculated by tumor volume at time intervals/the initial tumor volume×100%. The IR of tumor growth was calculated by the equation: IR= (mean tumor weight of control group−mean tumor weight of treatment group)/mean tumor weight of control group×100%. For an orthotopic model, MDA-MB-231 cells (4×10^6 (200 μL)$^{-1}$ PBS) were implanted into the mammary gland of female BALB/c nude mice (6–8 weeks). When tumors volume reached about 100 mm^3, mice (n=5) were treated with PEG-G3-PEITC/PTX or PEG-PDLLA/PTX micelles (eq. 10 mg kg^{-1} PTX) every other day. Body weight and tumor volume were recorded. All mice were euthanized after the completion of experiment. For histopathologic analysis, specimens of tumors and major organs (heart, liver, spleen, lung, and kidney) were fixed in 4% paraformaldehyde and embedded in paraffin. 5-μm-thick sections were cut and stained with haematoxylin/eosin (H&E) to assess histological profile. Sections were observed by light microscope (OLYMPUS, BX51, Japan).

In vivo real-time distribution

To visualize the real-time tissue distribution of micelles, BALB/c nude mice with *s.c.* MCF-7 tumors were *i.v.* injected with Cy5-labeled PEG-G3-PEITC/PTX or PEG-PDLLA/PTX micelles (eq. 10 mg kg^{-1} PTX). At 5 min and at 1, 2, 5, 8, 12, 24, and 36 h, mice were imaged under anesthesia with 1% sodium pentobarbital using a Kodak *In-Vivo* FX professional imaging system (Kodak, USA). Exposure time was 30 s per image.

Statistical analysis

Data are depicted as mean±SD. Two-tailed unpaired Student's t-test was used to test the statistical analysis. Difference was considered to be significant at the value of P<0.05.

Compliance and ethics *The author(s) declare that they have no conflict of interest.*

Acknowledgements *This work was supported by the National Natural Science Foundation of China (U1501243, 51603181), the National Basic Research Program (2014CB931900), the National Natural Science Foundation of China (51603181) and the Fundamental Research Funds for the Central Universities (2016QNA4024) for financial support.*

Berglund, M., Dalence-Guzman, M.F., Skogvall, S., and Sterner, O. (2008). SAR studies of capsazepinoid bronchodilators. Part 2: chlorination and catechol replacement in the A-ring. Bioorgan Med Chem 16, 2513–2528.

Burt, H.M., Zhang, X., Toleikis, P., Embree, L., and Hunter, W.L. (1999). Development of copolymers of poly(*D*,*L*-lactide) and methoxypolyethylene glycol as micellar carriers of paclitaxel. Colloids Surface B 16, 161–171.

Carstens, M.G., de Jong, P.H.J.L.F., van Nostrum, C.F., Kemmink, J., Verrijk, R., de Leede, L.G.J., Crommelin, D.J.A., and Hennink, W.E. (2008). The effect of core composition in biodegradable oligomeric micelles as taxane formulations. Eur J Pharm Biopharm 68, 596–606.

Chen, H., Kim, S., He, W., Wang, H., Low, P.S., Park, K., and Cheng, J.X. (2008). Fast release of lipophilic agents from circulating PEG-PDLLA micelles revealed by *in vivo* forster resonance energy transfer imaging. Langmuir 24, 5213–5217.

Fang, R.H., Aryal, S., Hu, C.M.J., and Zhang, L. (2010). Quick synthesis of lipid-polymer hybrid nanoparticles with low polydispersity using a single-step sonication method. Langmuir 26, 16958–16962.

Guo, Z., Zou, Y., He, H., Rao, J., Ji, S., Cui, X., Ke, H., Deng, Y., Yang, H., Chen, C., et al. (2016). Bifunctional platinated nanoparticles for photoinduced tumor ablation. Adv Mater 28, 10155–10164.

Gupta, P., Wright, S.E., Kim, S.H., and Srivastava, S.K. (2014). Phenethyl isothiocyanate: a comprehensive review of anti-cancer mechanisms. Biochim Biophys Acta 1846, 405–424.

Kim, S.C., Kim, D.W., Shim, Y.H., Bang, J.S., Oh, H.S., Kim, S.W., and Seo, M.H. (2001). *In vivo* evaluation of polymeric micellar paclitaxel formulation: toxicity and efficacy. J Control Release 72, 191–202.

Liu, K., Cang, S., Ma, Y., and Chiao, J.W. (2013). Synergistic effect of paclitaxel and epigenetic agent phenethyl isothiocyanate on growth inhibition, cell cycle arrest and apoptosis in breast cancer cells. Cancer Cell Int 13, 10.

Mishra, A., Dwivedi, J., Shukla, K., and Malviya, P. (2014). X-Ray diffr-

action and Fourier transformation infrared spectroscopy studies of copper (II) thiourea chloro and sulphate complexes. Journal of Physics Conference Series.
Muthoosamy, K., Abubakar, I.B., Bai, R.G., Loh, H.S., and Manickam, S. (2016). Exceedingly higher co-loading of curcumin and paclitaxel onto polymer-functionalized reduced graphene oxide for highly potent synergistic anticancer treatment. Sci Rep 6, 32808.
Saeed, A., Bolte, M., Erben, M.F., and Pérez, H. (2015). Intermolecular interactions in crystalline 1-(adamantane-1-carbonyl)-3-substituted thioureas with Hirshfeld surface analysis. Crystengcomm 17, 7551–7563.
Shao, S., Zhou, Q., Si, J., Tang, J., Liu, X., Wang, M., Gao, J., Wang, K., Xu, R., and Shen, Y. (2017). A non-cytotoxic dendrimer with innate and potent anticancer and anti-metastatic activities. Nat Biomed Eng 1, 7-45–757.
Singla, A.K., Garg, A., and Aggarwal, D. (2002). Paclitaxel and its formulations. Int J Pharm 235, 179–192.
Skog, S., He, Q., Khoshnoud, R., Fornander, T., and Rutqvist, L.E. (2004). Genes related to growth regulation, DNA repair and apoptosis in an oestrogen receptor-negative (MDA-231) versus an oestrogen receptor-positive (MCF-7) breast tumour cell line. Hum Hered 25, 41–47.
Stirland, D.L., Nichols, J.W., Miura, S., and Bae, Y.H. (2013). Mind the gap: a survey of how cancer drug carriers are susceptible to the gap between research and practice. J Control Release 172, 1045–1064.
Sun, Q., Radosz, M., and Shen, Y. (2012). Challenges in design of translational nanocarriers. J Control Release 164, 156–169.
Tang, B., Fang, G., Gao, Y., Liu, Y., Liu, J., Zou, M., and Cheng, G. (2014). Liprosomes loading paclitaxel for brain-targeting delivery by intravenous administration: *in vitro* characterization and *in vivo* evaluation. Int J Pharm 475, 416–427.
Tang, Z., He, C., Tian, H., Ding, J., Hsiao, B.S., Chu, B., and Chen, X. (2016). Polymeric nanostructured materials for biomedical applications. Prog Polymer Sci 60, 86–128.
Tyrrell, Z.L., Shen, Y., and Radosz, M. (2010). Fabrication of micellar nanoparticles for drug delivery through the self-assembly of block copolymers. Prog Polymer Sci 35, 1128–1143.
Wang, J., Sun, X., Mao, W., Sun, W., Tang, J., Sui, M., Shen, Y., and Gu, Z. (2013). Tumor redox heterogeneity-responsive prodrug nanocapsules for cancer chemotherapy. Adv Mater 25, 3670–3676.
Wang, Y.J., Wang, C., Gong, C.Y., Wang, Y.J., Guo, G., Luo, F., and Qian, Z.Y. (2012). Polysorbate 80 coated poly (-caprolactone)-poly (ethylene glycol)-poly (-caprolactone) micelles for paclitaxel delivery. Int J Pharm 434, 1–8.
Wei, Y., Li, L., Xi, Y., Qian, S., Gao, Y., and Zhang, J. (2014). Sustained release and enhanced bioavailability of injectable scutellarin-loaded bovine serum albumin nanoparticles. Int J Pharm 476, 142–148.
Wu, X., Zhou, Q., and Xu, K. (2009). Are isothiocyanates potential anticancer drugs? Acta Pharmacol Sin 30, 501–512.
Xi, X., Hu, S., Zhou, Z., Liu, X., Tang, J., and Shen, Y. (2016). Dendrimers with the protocatechuic acid building block for anticancer drug delivery. J Mater Chem B 4, 5236–5245.
Xiao, K., Luo, J., Fowler, W.L., Li, Y., Lee, J.S., Xing, L., Cheng, R.H., Wang, L., and Lam, K.S. (2009). A self-assembling nanoparticle for paclitaxel delivery in ovarian cancer. Biomaterials 30, 6006–6016.
Yano, S., Takehara, K., Kishimoto, H., Tazawa, H., Urata, Y., Kagawa, S., Bouvet, M., Fujiwara, T., and Hoffman, R.M. (2016). *In vivo* selection of intermediately- and highly- malignant variants of triple-negative breast cancer in orthotopic nude mouse models. Anticancer Res 36, 6-273–6278.
Zhang, P., Huang, Y., Liu, H., Marquez, R.T., Lu, J., Zhao, W., Zhang, X., Gao, X., Li, J., Venkataramanan, R., et al. (2014). A PEG-Fmoc conjugate as a nanocarrier for paclitaxel. Biomaterials 35, 7146–7156.
Zhang, P., Huang, Y., Kwon, Y.T., and Li, S. (2015). PEGylated fmoc-amino acid conjugates as effective nanocarriers for improved drug delivery. Mol Pharm 12, 1680–1690.
Zhao, B., Zhou, Z., and Shen, Y. (2016). Effects of chirality on gene delivery efficiency of polylysine. Chin J Polym Sci 34, 94–103.
Zhao, L., Zhou, Y., Gao, Y., Ma, S., Zhang, C., Li, J., Wang, D., Li, X., Li, C., Liu, Y., et al. (2015). Bovine serum albumin nanoparticles for delivery of tacrolimus to reduce its kidney uptake and functional nephrotoxicity. Int J Pharm 483, 180–187.
Zhou, Z., Ma, X., Jin, E., Tang, J., Sui, M., Shen, Y., Van Kirk, E.A., Murdoch, W.J., and Radosz, M. (2013). Linear-dendritic drug conjugates forming long-circulating nanorods for cancer-drug delivery. Biomaterials 34, 5722–5735.
Zhou, Z., Ma, X., Murphy, C.J., Jin, E., Sun, Q., Shen, Y., Van Kirk, E.A., and Murdoch, W.J. (2014). Molecularly precise dendrimer-drug conjugates with tunable drug release for cancer therapy. Angew Chem Int Ed 53, 10949–10955.
Zhou, Z., Liu, X., Zhu, D., Wang, Y., Zhang, Z., Zhou, X., Qiu, N., Chen, X., and Shen, Y. (2017). Nonviral cancer gene therapy: delivery cascade and vector nanoproperty integration. Adv Drug Deliver Rev 115, 115–154.
Zhu, A., Miao, K., Deng, Y., Ke, H., He, H., Yang, T., Guo, M., Li, Y., Guo, Z., Wang, Y., et al. (2015). Dually pH/reduction-responsive vesicles for ultrahigh-contrast fluorescence imaging and thermo-chemotherapy-synergized tumor ablation. ACS Nano 9, 7874–7885.

SUPPORTING INFORMATION

Figure S1 ^{1}H NMR spectra of PEG-G4-PEITC in DMSO-d_6.

Figure S2 The CMC values of polymers measured with a Nile red fluorescent method.

Figure S3 Stability of PEG-G3-PEITC/PTX micelles.

Figure S4 ^{1}H NMR spectra of PTX in $CDCl_3$, PEG-G3-PEITC in DMSO-d_6, and PEG-G3-PEITC/PTX micelles in D_2O.

Figure S5 Cytotoxicity of PEG-G3-PEITC blank micelles and PEG-PDLLA blank micelles.

Figure S6 Change of body weight.

Figure S7 Histopathologic analysis.

The supporting information is available online at http://life.scichina.com and https://link.springer.com. The supporting materials are published as submitted, without typesetting or editing. The responsibility for scientific accuracy and content remains entirely with the authors.